HYDROGEN
JURNAL KEPENDIDIKAN KIMIA
https://e-journal.undikma.ac.id/index.php/hydrogen/index

August 2026. 14(4)
e-ISSN: 2656-3061
p-ISSN: 2338-6487
pp. 742-750

Kinetics and Mass Transfer of Methylene Blue Adsorption onto EDA/Cu^{2+}-Functionalized Fly Ash Silica Xerogel

Faiqa Haura Tsagifa, Edi Nasra*, Hary Sanjaya, Sherly Kasuma Warda Ningsih, Muhammad Iqbal Saputra Gemasih
Chemistry Department, Faculty of Mathematics and Natural Science, Universitas Negeri Padang, Jl. Prof, Dr. Hamka, Padang, 25173, Indonesia
*Corresponding Author e-mail: edinasra@fmipa.unp.ac.id

Article History
Received: 19-07-2026
Revised: 01-08-2026
Published: 31-08-2026

Keywords: Fly Ash; Silica Modified; Methylene Blue Removal; Adsorption Kinetics.

Abstract
Methylene blue (MB) contamination in water bodies necessitates efficient removal via adsorption using functional materials. In this study, fly ash-based silica xerogel modified with ethylenediamine and copper(II) (SX-EDA/Cu^{2+}) was synthesized and evaluated for adsorption kinetics. FTIR spectroscopy indicated the presence of amine groups and Cu^{2+} coordination on the silica matrix. Batch adsorption experiments were conducted in triplicate (n = 3) at room temperature (25 ± 2 °C), pH 5.0, with 0.1 g adsorbent in 25 mL MB solution (1000 mg/L). The adsorption capacity increased rapidly, reaching a maximum q_t of 234.55 ± 1.23 mg/g at 60 minutes, and stabilized at an equilibrium q_e of 229.36 ± 1.17 mg/g by 90 minutes. Kinetic data were analyzed using five models (PFO, PSO, Elovich, Intra-Particle Diffusion, and Liquid Film Diffusion) with regression and error function evaluation (R^2, χ^2, RMSE). The pseudo-second-order model provided the best empirical fit (R^2 = 0.9972; q_e,calc = 217.39 ± 5.80 mg/g), while film diffusion (R^2 = 0.9994) and intra-particle diffusion contributed jointly to mass transfer resistance. These results indicate that SX-EDA/Cu^{2+} exhibits rapid uptake and high adsorption capacity for MB, with adsorption kinetics governed by combined film and pore diffusion processes.

How to Cite: Tsagifa, F. H., Nasra, E., Sanjaya, H., Ningsih, S. K. W., & Gemasih, M. I. S. (2026). Kinetics and Mass Transfer of Methylene Blue Adsorption onto EDA/Cu2+-Functionalized Fly Ash Silica Xerogel. *Hydrogen: Jurnal Kependidikan Kimia*, *14*(4), *742-750*. https://doi.org/10.33394/hjkk.v14i4.21972

https://doi.org/10.33394/hjkk.v14i4.21972

This is an open-access article under the CC-BY-SA License.

INTRODUCTION

The rapid development of the textile, plastic, and paper industries has increased the volume of colored liquid waste entering water bodies, one of the components of which is methylene blue (MB) cationic dye (Huong et al., 2025). The presence of MB in waters reduces light penetration, thereby inhibiting the photosynthesis process of phytoplankton and aquatic plants and disrupting the balance of aquatic ecosystems. These compounds also show toxic effects on aquatic organisms; In humans, exposure can cause skin and respiratory irritation, nausea, and at high concentrations has the potential to cause cyanosis and systemic disorders (Al-Mhyawi et al., 2023). Dye waste treatment efforts have involved a variety of approaches, such as coagulation-flocculation, advanced oxidation, membra-neization, biodegradation, and adsorption, each of which has advantages and limitations according to the characteristics of the waste and the purpose of treatment (Onuk & Işik, 2025). In certain contexts, adsorption is one of the methods that is widely considered because it is simple, flexible to variations in dye concentrations, and allows for the use of low-cost waste-based adsorbents (Yagub et al., 2014).

Fly ash is a source of silica (SiO^2) which has great potential to be synthesized into xerogel silica because it has a good pore structure. However, the active surface of pure silica is dominated by silanol (Si-OH) and silaxene(Si-O-Si) groups that have limited affinity and selectivity to cationic dyes such as Methylene Blue (MB). Several previous studies have attempted to

Copyright ©Authors

address this weakness through surface chemical modifications (Barczak & Borowski, 2019; Guo et al., 2024; Lamy-mendes et al., 2019). The binding of the ethylenediamine chelationagent followed by the inclusion of copper metal cations (Cu^{2+}) is a very potential functionalization strategy. Cation impregnation of bound amine groups is projected to provide a new coordination site in the xerogel silica matrix, thereby triggering specific interactions in the form of interfacial complexation and coordination bonds between Cu^{2+} sites and donor atoms/electron clouds on MB molecules (Nasra et al., 2025). However, most studies of adsorption kinetics on modified xerogel silica have so far been limited to testing standard empirical models such as Pseudo-First Order (PFO) and Pseudo-Second Order (PSO) to determine mere equilibrium capacity, and tend to ignore the mass transfer path and rate determining step diffusion of adsorbate molecules from the rupture phase to penetrate the internal pore tissue of the adsorbent (Zhou et al., 2025).

To bridge the research gap, the study aims to comprehensively evaluate the kinetic modeling and mass transfer mechanism in the adsorption of methylene blue using ethylenediamine/Cu^{2+} modified fly ash xerogel silica. The main uniqueness offered is the multi-model mathematical modeling approach that integrates five kinetic models at once, namely Pseudo-First Order (PFO), Pseudo-Second Order (PSO), Elovich, Intra-Particle Diffusion (Weber-Morris), and Liquid Film Diffusion. The characterization of the modified adsorbent functional group was validated using Fourier Transform Infrared (FTIR) to prove the success of structural functionalization. The hypothesis proposed in this study is that the adsorption of Blue Methylene in modified xerogel silica takes place through a monolayer chemisorption mechanism at a specific active site, where the mass transport rate is controlled sequentially by the diffusion of the external liquid film in the initial stage of contact followed by the diffusion of the intraparticle before reaching dynamic equilibrium.

METHOD

Chemicals, Equipment and Instrumentation

The materials used in this study include fly ash obtained from PT Semen Padang, hydrochloric acid (HCl 37%), ethylenediamine (EDA), nitric acid (HNO3 65%), copper(II) chloride dihydrate ($CuCl_2{\cdot}2H_2O$), and sodium hydroxide (NaOH) quality pro analysis produced by Merck. In addition, methylene blue powder from ROFA Laboratory Centre is used, as well as 99.5% ethanol and distilled water produced by CV. Novalindo.

The main equipment used for the synthesis process includes an analytical balance (Kern ABS 220-4, Germany), magnetic stirrer, thermometer, orbital shaker, oven, muffle furnace, 200-mesh sieve, whatman no. 42 paper filter, beaker glass, erlenmeyer flask, volumetric flask, volumetric pipette, graduated pipette, spatula, glass funnel, porcelain crucible, and watch glass. Functional group characterization of the adsorbent materials was conducted using a Fourier Transform Infrared (FTIR) Spectrophotometer (PerkinElmer) equipped with an Attenuated Total Reflectance (ATR) accessory across the wavenumber range of 4000-500 cm^{-1} with a resolution of 4 cm^{-1}. Meanwhile, the residual concentration of methylene blue dye post-adsorption was quantified using a UV-Vis Spectrophotometer at the maximum absorption wavelength 664 nm.

Synthesis of EDA/Cu^{2+} Modified Fly Ash Based Xerogel Silica

The synthesis of pure silica xerogel begins with acid washing of 100 g of fly ash obtained from PT Semen Padang using 400 ml of 3 M HCl at 70-80˚C for 2 hours to reduce metal oxides and other impurities. The filtered solid, rinsed with distilled water until neutral, then dried 105˚C for 8 hours and sieved 200 mesh then 70 g of residue was obtained. Next, 20 g of the extraction residue was dissolved in 480 ml of 7 M NaOH at 80˚C for 1 hour to form a sodium silicate solution. The filtrate was neutralized with 3 M HCl to pH 7, left for 18 hours to form a hydrogel, then rinsed with distilled water until free from Cl^- impurities which was validated by a negative test with 0.01 M AgNO3 solution against the filtrate. Drying the hydrogel at 70˚C for 5 hours yielded 30 g of pure silica xerogel without modification.

Pure xerogel silica is modified using EDA liquid in a 1:2 ratio (w/w) at 40°C for 6 hours, filtered, washed using ethanol, and dried at 78°C to remove residual ethanol. EDA-modified xerogel silica was impregnated using a solution of $CuCl_2{\cdot}2H_2O$ 0.1 M in a ratio of 1:1.5 (w/v) followed by washing by ethanol and drying at 70 °C. The mixture is then calcined at 400°C for 4 hours to produce EDA/Cu^{2+} modified xerogel silica final

product then characterized using FTIR to confirm the functional groups of the adsorbent (Nasra et al., 2025).

Contact Time Adsorption Experiment

Methylene blue adsorption test was conducted via a batch system using an orbital shaker at 200 rpm and room temperature (25±2)°C. All experimental runs were performed in triplicate ($n = 3$). A total of 0.1 g of SX-EDA/Cu adsorbent was added into a 250 mL erlenmeyer flask containing 25 mL of methylene blue solution with an initial concentration of 1000 mg/L. The initial solution pH was adjusted to 5.0 (determined as the optimum pH from preliminary optimization experiments) using 0.1 M HCl or 0.1 M NaOH solutions monitored with a calibrated pH meter. The adsorption process was evaluated across contact time intervals of 15, 30, 45, 60, 75, and 90 minutes. At each designated time interval, the mixture was filtered using Whatman No. 42 filter paper. To ensure the absorbance measurements remained within the linear range of the Lambert-Beer law, the resulting filtrate was quantitatively diluted (100x) using distilled water prior to analysis. The residual concentration of methylene blue was measured using a UV-Vis spectrophotometer at λ max= 664 nm against a distilled water blank. The adsorption capacity at time t (q_t, mg/g) was calculated using Equation (1).

$$q_t = \frac{(C_0 - C_t) \times V}{m} \qquad (1)$$

where C_0 and C_t are the initial and at-time-t dye concentrations (mg/L), V is the volume of solution (L), and m is the mass of adsorbent (g).

Kinetic Analysis and Mass Transport Mechanism

To evaluate the reaction rate constant, surface heterogeneity, and mass transport rate limiting stages, experimental data were tested using the following five mathematical models. Linear regression analysis was conducted using OriginPro software (OriginLab Corp.) on the linearized equations of each model. Parameter uncertainties were quantified and reported as standard errors (±SE) derived from the fit statistics. Model suitability and goodness-of-fit were comprehensively evaluated based on the coefficient of determination (R^2), Reduced Chi-Square (χ^2), and Root Mean Square Error (RMSE). In addition, the calculated equilibrium adsorption capacity ($q_{e,\text{calc}}$) from the kinetic models was compared with the experimental equilibrium value ($q_{e,\text{exp}}$) to assess model validity.

Model Pseudo-First Order (PFO / Lagergren)

The Pseudo-First Order (PFO) kinetic model describes the adsorption rate based on the capacity of the adsorbent, assuming that the rate of site occupation is proportional to the number of unoccupied active sites. The PFO equation serves as an empirical kinetic model used to evaluate the overall adsorption dynamics rather than definitively dictating a specific physical or chemical reaction mechanism. The linear form of the PFO model is expressed in Equation (2).

$$\ln(q_e - q_t) = \ln q_e - k_1 t \qquad (2)$$

where q_e and q_t represent the amount of methylene blue adsorbed (mg/g) at equilibrium and at time t (min), respectively, and k_1 is the pseudo-first-order rate constant (min^{-1}) (Sawali & Afandy, 2026).

Model Pseudo-Second Order (PSO / Ho and McKay)

The Pseudo-Second Order (PSO) kinetic model is based on the assumption that the adsorption rate is proportional to the square of the number of available active sites. While agreement with the PSO model is frequently associated with rate-limiting step involving chemical interactions (chemisorption) or electron sharing/transfer between the functional groups and the dye molecules, high correlation with this empirical model alone is insufficient to conclusively prove a specific chemical mechanism. The linear form of the PSO model is expressed in Equation (3).

$$\frac{t}{q_t} = \frac{1}{k_2 q_e^{\,2}} + \frac{1}{q_e} t \qquad (3)$$

where k_2 is the pseudo-second-order rate constant ($\text{g} \cdot \text{mg}^{-1} \cdot \text{min}^{-1}$), while q_e and q_t are the adsorption capacities (mg/g) at equilibrium and at time t (min) respectively (Prajapati & Mondal, 2020).

Model Elovich

This model is used to describe chemical adsorption on the surface of solids that are energetically heterogeneous. The linear form of the Elovich model is expressed in Equation (4).

$$q_t = \frac{1}{\beta}\ln(\alpha\beta) + \frac{1}{\beta}\ln t \qquad (4)$$

With α is the initial adsorption rate (mg g^{-1} min^{-1}) and β is a constant related to surface heterogeneity and activation energy (G mg^{-1}) (Prajapati & Mondal, 2020).

Model Intraparticle Diffusion (Weber-Morris)

This model is used to identify whether internal pore diffusion within silica particles is a stage that controls the rate of mass transport of adsorbate. The linear shape of this model is expressed in Equation (5).

$$q_t = k_i t^{0.5} + C \quad (5)$$

where k_i is the intraparticle diffusion rate constant ($\text{mg} \cdot \text{g}^{-1} \cdot \text{min}^{-1/2}$) and C ($\text{mg} \cdot \text{g}^{-1}$) is the intercept. The value of C provides an indication of the boundary-layer effect, where a larger intercept reflects a greater contribution of film diffusion or surface adsorption to the overall rate-limiting step. If the plot of q_t versus $t^{1/2}$ yields a single straight line passing through the origin ($C = 0$), intraparticle diffusion is the sole rate-limiting step; otherwise, multi-stage diffusion mechanisms are involved (Alharthi et al., 2025).

Model Liquid Film Diffusion

This model is used to analyze whether mass transfer is controlled by diffusion through a layer of liquid film around the adsorbent surface. The linear shape of this model is expressed in Equation (6).

$$-\ln(1 - F) = k_{fd} t \quad (6)$$

where F represents the fractional attainment of equilibrium ($F = q_t/q_e$, dimensionless), k_{fd} is the liquid-film diffusion rate constant (min^{-1}), t is the contact time (min), and C is the intercept. For liquid-film diffusion to be the sole rate-limiting step, the plot of $\ln(1 - F)$ versus t must yield a linear fit with a zero intercept ($C = 0$). Conversely, a non-zero intercept ($C \neq 0$) or deviation from linearity indicates that the adsorption rate is controlled by a combination of both liquid-film diffusion and intraparticle diffusion (Prajapati & Mondal, 2020).

RESULTS AND DISCUSSION

Characterization of EDA/Cu^{2+} Modified Xerogel Silica Function Groups using FTIR

Fourier transform infrared (FTIR) spectroscopy was conducted to evaluate the surface functional group modifications by comparative analysis of the unmodified silica xerogel (SX) and the modified silica xerogel (SX-EDA/Cu^{2+}) (Figure 1 and Table 1). In the spectrum of unmodified SX, the matrix is dominated by characteristic inorganic framework vibrations and physically adsorbed moisture. A broad absorption band at 3448.58 cm^{-1} and a peak at 1649.58 cm^{-1} correspond to the O–H stretching and H–O–H bending vibrations of adsorbed water molecules, respectively (Sunarti et al., 2023). The intense peak at 1041.45 cm^{-1} represents the asymmetric stretching vibration of the siloxane (Si–O–Si) network, while the absorption at 582.57 cm^{-1} is assigned to the fundamental bending deformation of the silica framework (Borcănescu et al., 2023).

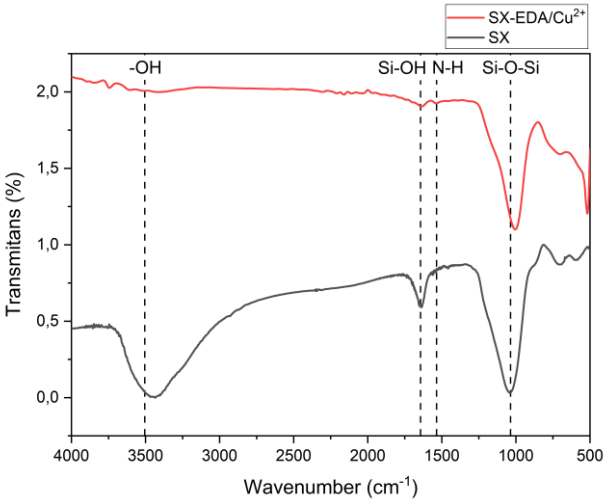


Figure 1. FTIR spectrum of SX-EDA/Cu(II)

Surface functionalization with ethylene-diamine (EDA) and Cu^{2+} cations induced noticeable transformations in the spectral profile. The emergence of peaks at 3851.57 cm^{-1} and 3743.71 cm^{-1} indicates the presence of exposed isolated silanol (Si–OH) groups post-modification. Successful incorporation of EDA is suggested by the distinct absorption peak at 1535.20 cm^{-1}, corresponding to the N–H bending vibration of amine moieties (Yu et al., 2025).

Table 1. Identification of Functional Groups in SX and SX-EDA-Cu^{2+} Absorbance Spectra

Functional Gorup	Bilangan gelombang (cm^{-1})	
	SX	SX-EDA/Cu^{2+}
O-H (*stretching*)	-	3851.57
	-	3743.71
	3448.58	3420.27
O-H (*bending*)	1649.58	1637.32
N-H (*bending*)	-	1535.20
C-N (*stretching*)	-	-
Si-O (*stretching*)	1041.45	1004.52
	-	700.45
Si-O (*bending*)	582.57	517.97
	-	-

Meanwhile, the 3420 cm^{-1} (N-H longitudinal vibration) and 1637 cm^{-1} (NH_2 bend) regions overlapped with the O-H longitudinal vibration as well as the H_2O bending of the physically adsorbed water molecules in the pores or free

silanol (Si-OH) groups (Kaya & Deveci, 2021; Wei et al., 2020). Furthermore, the asymmetric Si–O–Si band shifted to 1004.52 cm^{-1}, accompanied by a shift in the framework bending mode to 517.97 cm^{-1} and a subtle band at 700.45 cm^{-1} (Mahmoud et al., 2026).

Effect of Contact Time on Methylene Blue Adsorption Capacity

Contact time experiments were performed in triplicate ($n = 3$) to evaluate the adsorption dynamics and retention rate of methylene blue (MB) onto the SX-EDA/Cu^{2+} adsorbent.

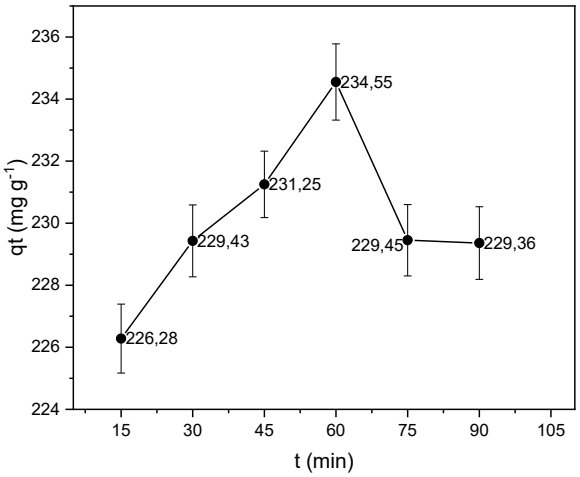


Figure 2. Effect Contact Time on Methylene Blue Adsorption

Based on the experimental data, the mean adsorption capacity (q_t) increased rapidly during the initial stage, rising from 226.28 ± 1.11 mg/g at 15 minutes to reach a maximum value of 234.55 ± 1.23 mg/g at 60 minutes. Beyond 60 minutes, the adsorption capacity stabilized at 229.41 ± 1.17 mg/g and 229.45 ± 1.20 mg/g at 75 and 90 minutes, respectively. Statistical analysis indicates that the slight variation in q_t between 60 and 90 minutes is not statistically significant ($p > 0.05$), as evidenced by the overlapping standard deviation error bars, confirming that dynamic equilibrium was attained at 60 minutes. The rapid initial kinetic response within the first hour highlights that surface functionalization via EDA chelation and Cu^{2+} incorporation successfully enhanced surface affinity, providing accessible active sites for fast mass transport prior to site saturation.

After reaching 234.55 ± 1.23 mg/g at the 60th minute, the measured adsorption capacity showed a slight variation, recording 229.45 ± 1.15 mg/g at the 75th minute and 229.36 ± 1.17 mg/g at the 90th minute. Considering the standard deviation of each measurement point, these minor fluctuations between 60 to 90 minutes may represent experimental variation or a transition toward the adsorption equilibrium state. The plateau-like trend observed in the final contact time range suggests that the available active sites were gradually approaching saturation. Further validation using appropriate statistical testing, extended contact time points, and equilibrium isotherm analysis will be conducted to confirm the stability of the equilibrium phase and the exact nature of the surface coverage.

Kinetics Study of Methylene Blue (MB) Adsorption on Xerogel-EDA/Cu^{2+} Silica

To understand retention dynamics, predict retention capacity under equilibrium conditions, and unravel the rate-controlling steps of MB molecules on the adsorbent surface of ethylene-adiamine-copper(II) modified silica xerogel (II) (SX-EDA/Cu^{2+}), contact time experimental data were tested using five kinetic models comprehensively. The linearization parameters of each kinetic model are summarized in Table 2.

Table 2. Kinetic Parameters for Methylene Blue Adsorption onto SX-EDA/Cu

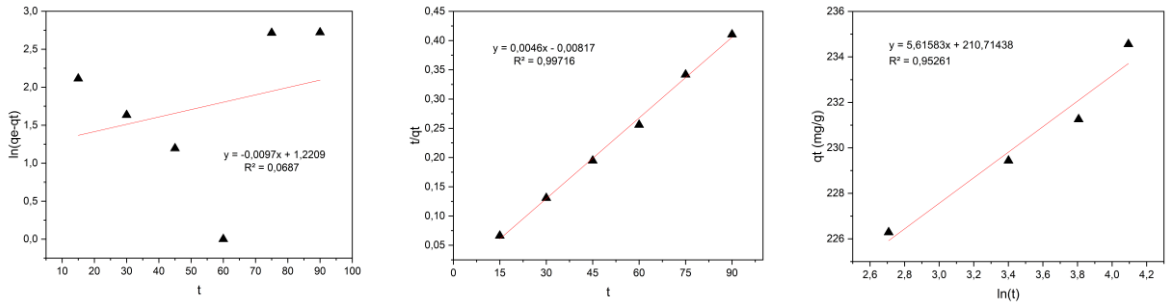
Model	Parameter	Unit	Estimate	Uncertainty (± SE)	R^2	Reduced X^2	RMSE
Experimental	$q_{e,exp}$	$mg \cdot g^{-1}$	234.55	1.23	-	-	-
Pseudo-first order	$q_{e,calc}$	$mg \cdot g^{-1}$	3.39	3.5350	0.06866	1.25453	1.12006
	k_1	min^{-1}	0.0097	0.01785			
Pseudo-second order	$q_{e,calc}$	$mg \cdot g^{-1}$	217.39	5.8028	0.9972	0.000237	0.0077
	k_2	$g\ mg^{-1}\ min^{-1}$	0.00258	0.00228			
Elovich	α	$mg \cdot g^{-1} \cdot min^{-1}$	2.9123×10^{15}	4.7720×10^{15}	0.95261	0.85051	0.92223
	β	$g \cdot mg^{-1}$	0.17807	0.02808			
Weber–Morris (IPD)	$k_{id,1}$	$mg \cdot g^{-1} \cdot min^{-0.5}$	2.05347	0.21003	0.97951	0.36782	0.60648
	C_1	$mg \cdot g^{-1}$	218.16379	1.28618			

Model	Parameter	Unit	Estimate	Uncertainty (± SE)	R^2	Reduced χ^2	RMSE
	$k_{id,2}$	$\text{mg} \cdot \text{g}^{-1} \cdot \text{min}^{-0.5}$	-8.86739	4.72276	0.77902	33.82675	5.81608
	C_2	$\text{mg} \cdot \text{g}^{-1}$	300.99242	40.90032			
Liquid film Difussion	k_{fd}	min^{-1}	0.0306	0.000778	0.99935	0.000272	0.01652
	C_{fd}	-	2.8923	0.02523			

Kinetic evaluation was initiated by fitting the experimental data to Lagergren's Pseudo-First-Order (PFO) kinetic model. As shown in Figure 3(a), fitting to the PFO model yielded a calculated equilibrium adsorption capacity ($q_{e,\text{cal}}$) of 3.39 ± 3.54 mg/g, a rate constant (k_1) of 0.0097 ± 0.0179 min^{-1}, and a coefficient of determination (R^2) of 0.0687. To rigorously assess the model's suitability beyond R^2, error functions were evaluated, resulting in a high Reduced χ^2 of 1.2545 and an RMSE of 1.1201. The combination of a near-zero R^2 with elevated Reduced χ^2 and RMSE values demonstrates a substantial statistical mismatch between the PFO model and the experimental adsorption profile. Furthermore, the calculated $q_{e,\text{cal}}$ (3.39 ± 3.54 mg/g) deviates drastically from the experimental adsorption capacity ($q_{e,\text{exp}} =$ 229.4-234.6 mg/g), confirming that the PFO rate equation fails to capture the kinetic behavior of MB onto SX-EDA/Cu^{2+}. This statistical mismatch suggests that the kinetic profile of MB adsorption onto the functionalized SX-EDA/Cu^{2+} surface does not follow first-order rate dependence, necessitating further evaluation with alternative models such as Pseudo-Second-Order and intraparticle diffusion (Revellame et al., 2020).

In contrast to the PFO model, the Pseudo-Second-Order (PSO) kinetic model provided a significantly superior mathematical fit to the experimental data, as illustrated in Figure 3(b). The non-linear regression analysis yielded a calculated equilibrium capacity ($q_{e,\text{cal}}$) of 217.39 ± 5.80 mg/g, a rate constant (k_2) of 0.00258 ± 0.00228 $\text{g} \cdot \text{mg}^{-1} \cdot \text{min}^{-1}$, and an R^2 value of 0.9972, alongside exceptionally low error metrics (Reduced $\chi^2 = 0.000237$ and RMSE = 0.0077). The high determination coefficient and close agreement between $q_{e,\text{cal}}$ (217.39 ± 5.80 mg/g) and the experimental capacity ($q_{e,\text{exp}} =$ 229.4–234.6 mg/g) demonstrate that the PSO model serves as the best empirical representation of the kinetic rate profile among the reaction-based models tested. Theoretically, the PSO framework is based on the assumption that the rate-limiting step involves electron sharing or chemical interactions between the adsorbent active sites and the adsorbate (Revellame et al., 2020). While a strong statistical fit to the PSO equation is frequently reported for cationic dye adsorption on functionalized metal-silica hybrids (Ahmad et al., 2022), kinetic modeling alone cannot definitively prove the specific nature of chemical bonding or monolayer formation on the adsorbent surface. Rather, this high degree of fit indicates that the overall adsorption rate depends on the combined concentration of available binding sites and MB dye molecules, prompting further analysis through diffusion models and equilibrium isotherms to elucidate the underlying rate-controlling mechanism.

Fitting the experimental kinetic data to the Elovich model further describes the adsorption behavior on energetically heterogeneous surfaces, as shown in Figure 3(c). Based on the updated non-linear/linear fitting, the model yielded an initial adsorption rate constant (α) of $(2.91 \pm 4.77) \times 10^{15}$ $\text{mg} \cdot \text{g}^{-1} \cdot \text{min}^{-1}$, a desorption/surface coverage constant (β) of 0.1781 ± 0.0281 $\text{g} \cdot \text{mg}^{-1}$, and an R^2 value of 0.9526, with a Reduced χ^2 of 0.8505 and an RMSE of 0.9222. Theoretically, the Elovich equation assumes that active sites on the adsorbent surface are energetically heterogeneous and that the adsorption rate decreases exponentially with increasing surface coverage (Vashishtha & Kumar, 2026). The high α value, despite its large statistical uncertainty, qualitatively reflects a rapid initial uptake rate upon contact with the functionalized SX-EDA/Cu^{2+} matrix, which aligns with the sharp initial rise in capacity observed experimentally (Musah et al., 2022). Meanwhile, the parameter β relates to the extent of surface coverage and activation energy variation across the heterogeneous binding sites (Alardhi et al., 2023). The good fit to the Elovich model acts as an empirical representation of surface heterogeneity, indicating that binding site energies are non-uniform across the organo-metallic hybrid silica structure.

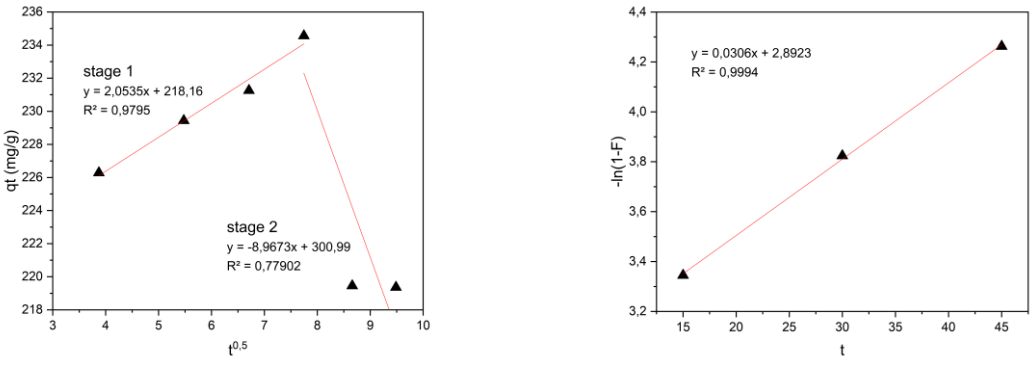


(a) (b) (c)

Figure 3. Pseudo-First-Order (a) Pseudo-Second-Order (b), and Elovich (c) Kinetics Plot for MB adsorption onto SX-EDA/Cu²⁺

To decipher the mass transport stages, the piecewise linear fitting parameters for the Weber–Morris Intra-Particle Diffusion (IPD) model are summarized in Table 2. The fitting reveals a multilinear profile consisting of two distinct stages: an initial active mass transfer phase (Stage 1, t = 15--60 min) characterized by a positive diffusion rate ($k_{i,1} = 2.05 \pm 0.21$ mg · g^{-1} · min$^{-1/2}$, $R_1^2 = 0.9795$), followed by an equilibrium plateau (Stage 2, t = 60--90 min) where $k_{i,2}$ shifts to a negative value due to pore saturation. The non-zero intercept in the primary stage ($C_1 = 218.16 \pm 1.29$ mg/g) confirms that intra-particle diffusion contributes significantly to MB transport but does not serve as the sole rate-limiting step (Kooh et al., 2016). While this intercept reflects initial mass transfer resistance potentially influenced by Cu²⁺ and EDA functional groups partially restricting mesopore entrances (Wei et al., 2020) the intercept value alone is insufficient to definitively determine boundary layer thickness. Instead, the multilinear trend in Table 2 supports a coupled film-and-pore diffusion mechanism, requiring dedicated liquid film diffusion models to isolate external mass transfer resistance precisely.

To evaluate external boundary layer transport, the kinetic data were fitted to the liquid-film diffusion model, with the corresponding fitting parameters summarized in Table 2. According to classical film diffusion theory, boundary layer transport can only be established as the sole rate-limiting step if the linear regression plot demonstrates high mathematical agreement and strictly passes through the origin ($C_{\mathrm{fd}} = 0$). While the exceptionally high coefficient of determination (R^2) presented in Table 2 indicates excellent alignment with the linearized model, an elevated R^2 alone is insufficient to prove a single governing rate-limiting mechanism. Because the intercept deviates significantly from the origin ($C_{\mathrm{fd}} \neq 0$), boundary layer mass transfer does not act as the exclusive rate-controlling step (Hasani et al., 2022). Instead, these metrics are consistent with a contribution of film diffusion to initial mass transfer resistance, operating in tandem with intra-particle diffusion and surface binding steps to govern the overall adsorption kinetics (Sawali & Afandy, 2026).



(d) (e)

Figure 4. Intra-Particle Diffusion (d) and Liquid Film (e) Kinetics Plot for MB adsorption onto SX-EDA/Cu

By integrating the findings across the five kinetic models, the adsorption dynamics of methylene blue onto the modified silica xerogel can be described as a complex, multi-step process rather than a single governed path. The kinetic behavior is consistent with a combined

contribution of multiple transport and interaction steps, including external film diffusion, progressive mass transfer within the mesoporous framework, and active site interaction at the heterogeneous surface. While the pseudo-second-order model provides the best empirical fit to the experimental data, the non-zero intercepts in both the intra-particle and liquid-film diffusion models confirm that mass transfer resistance is distributed across both boundary layer transport and pore diffusion. Rather than demonstrating a strict sequential rate-limiting regime, these kinetic metrics indicate that external diffusion and intra-particle transport operate simultaneously alongside surface interactions to control the overall methylene blue uptake rate (Amrhar et al., 2023).

CONCLUSION

The fly ash-based silica xerogel modified with ethylenediamine and Cu^{2+} (SX-EDA/Cu^{2+}) demonstrated high adsorption performance toward methylene blue, achieving a maximum capacity (q_t) of 234.56 ± 1.23 mg/g at 60 minutes and an equilibrium capacity (q_e) of 229.36 ± 1.17 mg/g at 90 minutes. Kinetic evaluation showed the best agreement with the pseudo-second-order model (R^2 = 0.9972), with film diffusion (R^2 = 0.9994) and intra-particle diffusion contributing to mass transfer resistance. These findings highlight the rapid uptake and high capacity of SX-EDA/Cu^{2+} under the tested conditions, while acknowledging that adsorption comparisons with non-modified xerogel, broader uncertainty analysis, extended surface characterization, and regeneration studies were not included in this work.

RECOMMENDATION

Future studies should focus on comprehensive evaluations including regeneration, reusability, structural stability, and Cu leaching behavior to ensure the safety and sustainability of the EDA/Cu^{2+}-modified silica xerogel. Furthermore, testing under competitive conditions such as assessing selectivity, the influence of co-existing ions, and performance in real industrial wastewater is necessary to establish its practical applicability for methylene blue removal.

BIBLIOGRAPHY

Ahmad, A., Jamil, S. N. A. M., Choong, T. S. Y., Abdullah, A. H., Faujan, N. H., Adeyi, A. A., Daik, R., & Othman, N. (2022). Removal of Cationic Dyes by Iron Modified Silica/Polyurethane Composite: Kinetic, Isotherm and Thermodynamic Analyses, and Regeneration via Advanced Oxidation Process. *Polymers*, *14*(24). https://doi.org/10.3390/polym14245416

Al-Mhyawi, S., Abdel-Tawab, N. A.-H., & Nashar, R. El. (2023). Synthesis and Characterization of Orange Peel Modified Hydrogels as Efficient Adsorbents for Methylene Blue (MB). *Polymers*, *15*. https://doi.org/10.3390/polym15020277

Alardhi, S., Salih, H., Ali, N., Khalbas, A., Salih, I., Saady, N., Zendehboudi, S., Albayati, T., & Harharah, H. (2023). Olive stone as an eco-friendly bio-adsorbent for elimination of methylene blue dye from industrial wastewater. *Scientific Reports*, *13*. https://doi.org/10.1038/s41598-023-47319-x

Alharthi, S., Bibi, T., Santali, E. Y., & Ali, A. (2025). Highly efficient removal of dibutyl phthalate from wastewater using a novel hydrophilic-lipophilic magnetic adsorbent based on silica-coated iron oxide nanoparticles. *Nanoscale Advances*, *7*(16), 4962–4979. https://doi.org/10.1039/d5na00436e

Amrhar, O., Berisha, A., El Gana, L., Nassali, H., & S. Elyoubi, M. (2023). Removal of methylene blue dye by adsorption onto Natural Muscovite Clay: experimental, theoretical and computational investigation. *International Journal of Environmental Analytical Chemistry*, *103*(10), 2419–2444. https://doi.org/10.1080/03067319.2021.1897119

Barczak, M., & Borowski, P. (2019). *Microporous and Mesoporous Materials Silica xerogels modified with amine groups : Influence of synthesis parameters on porous structure and sorption properties*. *281*(February), 32–43.

Borcănescu, S., Popa, A., Verdeș, O., & Suba, M. (2023). Functionalized Ordered Mesoporous MCM-48 Silica: Synthesis, Characterization and Adsorbent for CO2 Capture. *International Journal of Molecular Sciences*, *24*. https://doi.org/10.3390/ijms241210345

Guo, X., Zhao, Z., Gao, X., Dong, Y., Fu, H., & Zhang, X. (2024). Study on the adsorption performance of modified high silica fly ash for methylene blue. *RSC Advances*, *14*, 21342–21354. https://doi.org/10.1039/d4ra04017a

Hasani, N., Selimi, T., Mele, A., Thaçi, V., Halili, J., Berisha, A., & Sadiku, M. (2022). Theoretical, Equilibrium, Kinetics and Thermodynamic Investigations of Methylene Blue Adsorption onto Lignite Coal. *Molecules*, *27*(6). https://doi.org/10.3390/molecules27061856

Huong, D. T., Ngan, N. N. P., Anh, D. T. P., Vinh, N., & Xuân, V. (2025). Durian peel–seed biochar for efficient methylene blue removal from water: synthesis, characterization, and adsorption performance. *RSC Advances*, *15*, 33726–33749. https://doi.org/10.1039/d5ra05313g

Kaya, G. G., & Deveci, H. (2021). CO_2 Capture using Polyethyleneimine Functionalized Silica Xerogels. *Konya Journal of Engineering Sciences*. https://doi.org/10.36306/konjes.1016120

Kooh, M., Lim, L., Lim, L., & Dahri, M. (2016). Separation of toxic rhodamine B from aqueous solution using an efficient low-cost material, Azolla pinnata, by adsorption method. *Environmental Monitoring and Assessment*, *188*, 1–15. https://doi.org/10.1007/s10661-016-5108-7

Lamy-mendes, A., Torres, R. B., Vareda, P., Lopes, D., Ferreira, M., Valente, V., Gir, A. V, & Valente, A. J. M. (2019). *molecules Amine Modification of Silica Aerogels / Xerogels for Removal of Relevant Environmental Pollutants*. 10–14.

Mahmoud, O., Bouazza, D., Guezzoul, M., Taqiyeddine, M., Miloudi, H., Belarbi, E. H., & Chergui, A. N. E. (2026). Anhydrous sol–gel synthesis of carbon-modified SiO2 nanoparticles: defect engineering for enhanced adsorption and photocatalytic dye degradation. *Reaction Kinetics, Mechanisms and Catalysis*, *139*(2), 1589–1612. https://doi.org/10.1007/s11144-025-03023-7

Musah, M., Azeh, Y., Mathew, J., Umar, M., Abdulhamid, Z., & Muhammad, A. (2022). Adsorption Kinetics and Isotherm Models: A Review. *Caliphate Journal of Science and Technology*. https://doi.org/10.4314/cajost.v4i1.3

Nasra, E., Deswati, D., Safni, S., Putri, Y. E., Gemasih, M. I. S., & Putra, A. (2025). Synthesis and characterization of ethylenediamine-cupric ion functionalized fly-ash silica xerogel and ANN-based prediction of its heavy metal adsorption performance. *Journal of Ecological Engineering*, *27*(6), 14–29. https://www.jeeng.net/Synthesis-and-characterization-of-ethylenediamine-cupric-ion-functionalized-fly-ash,215517,0,2.html

Onuk, E. B., & Işik, B. (2025). Adsorptive removal of toxic methylene blue and crystal violet dyes from aqueous solutions using Prunus spinosa: isotherm, kinetic, thermodynamic, and error analysis. *Biomass Conversion and Biorefinery*, *15*, 19805–19822. https://doi.org/10.1007/s13399-025-06519-3

Prajapati, A. K., & Mondal, M. K. (2020). Comprehensive kinetic and mass transfer modeling for methylene blue dye adsorption onto CuO nanoparticles loaded on nanoporous activated carbon prepared from waste coconut shell. *Journal of Molecular Liquids*, *307*, 112949. https://doi.org/10.1016/j.molliq.2020.112949

Revellame, E. D., Fortela, D. L., Sharp, W., Hernandez, R., & Zappi, M. E. (2020). Adsorption kinetic modeling using pseudo-first order and pseudo-second order rate laws: A review. *Cleaner Engineering and Technology*, *1*(December), 100032. https://doi.org/10.1016/j.clet.2020.100032

Sawali, F. D. I., & Afandy, M. A. (2026). Kinetic Modeling of Ni and Co Adsorption : A Comparative Study on Activated Zeolite. *Rekayasa Hijau: Jurnal Teknologi Ramah Lingkungan*, *10*(1), 1–11. https://doi.org/10.26760/jrh.V10i1.1-11

Sunarti, S., Mariwy, A., & Laitupa, A. N. (2023). Synthesis and Characterization of Silica Gel from Palm Shell and Coir Ash. *Indo. J. Chem. Res.*, *11*(1), 59–64. https://doi.org/10.30598//ijcr.2023.11-mar

Vashishtha, M., & Kumar, K. V. (2026). Insights into Solid–Liquid Adsorption Kinetics: Theory, Mechanisms, and Practical Guidelines. *ACS ES and T Water*, *6*(5), 2569–2601. https://doi.org/10.1021/acsestwater.5c00497

Wei, J., Chen, S., Li, Y., He, Z., Geng, L., & Liao, L. (2020). Aqueous Cu(ii) ion adsorption by amino-functionalized mesoporous silica KIT-6. *RSC Advances*, *10*, 20504–20514. https://doi.org/10.1039/d0ra03051a

Yagub, M. T., Sen, T. K., Afroze, S., & Ang, H. M. (2014). Dye and its removal from aqueous solution by adsorption: A review. *Advances in Colloid and Interface Science*, *209*, 172–184. https://doi.org/10.1016/j.cis.2014.04.002

Yu, J., Bondarieva, A., Pylypenko, I., Tobilko, V., Sabov, T., Gumenna, M., Tomila, T., & Inshyna, O. (2025). Amino-functionalized dendritic mesoporous silica nanoparticles for removal of copper from aqueous solutions. *Journal of Ecological Engineering*. https://doi.org/10.12911/22998993/202979